






Electrostatic screening in a wire medium

Eugene Koreshin ^{*}, Ivan Matchenya , Grigoriy Karsakov, Denis Ilin , Ivan Iorsh, and Pavel Belov 
 ITMO University, St. Petersburg 197101, Russia

 (Received 23 November 2022; revised 16 March 2023; accepted 20 March 2023; published 30 March 2023; corrected 4 April 2023)

We extensively study screening in anisotropic artificial media formed by arrays of parallel metal wires both analytically and experimentally. Our findings show that the electrostatic potential distribution produced by probe charge is spherically symmetrical in the vicinity of the source. We also derive a boundary condition for the wire medium and confirm its validity experimentally. Despite the finite dimensions of the wire arrays, the field symmetry near the charge remains unaffected, but a local maximum potential is produced at the boundary. The screening depth of the wire medium is determined by its geometrical parameters and is proportional to the plasma frequency, which leads us to propose an experimental method for defining plasma frequency through static E-field measurement.

DOI: [10.1103/PhysRevB.107.115170](https://doi.org/10.1103/PhysRevB.107.115170)

I. INTRODUCTION

It is widely appreciated that static dielectric screening leads to substantial modification of Coulomb interaction potential in nanostructured and low-dimensional media. Probably one of the most famous examples is the Keldysh-Rytova potential [1,2] emerging due to static dielectric screening in thin semi-conducting film, which drastically affects electronic transport and optical properties in low-dimensional materials such as graphene and transition metal dichalcogenides [3,4]. Electrostatic screening also plays a crucial role in nanostructured media such as solutions, gels, and colloidal crystals [5–9].

At the same time, the idea that one can control transport properties by the artificial engineering of electrostatic screening is relatively new, and has so far been mostly developed in the context of two-dimensional materials and van der Waals heterostructures. This is rather surprising, since the methods to control dynamical fields, electromagnetic radiation by nanostructuring, have been thoroughly explored, which lead to the emergence of the now-established area of metamaterials [10,11].

In this article, we will consider an electrostatic response of paradigmatic metamaterial wires—a so-called wire medium [12]. This is an artificial material formed by long parallel metal wires periodically arranged in a square grid [Fig. 1(a)]. In the long wavelength limit the dielectric permittivity tensor of the wire medium is nonlocal and diagonal with components given by [13]

$$\varepsilon(\omega, k_z) = \text{diag} \left[1, \quad 1, \quad 1 - \frac{k_p^2}{k_0^2 - k_z^2} \right], \quad (1)$$

where $k_0 = \omega/c$ is the free space wave vector; k_p is the effective plasma wave vector, which is defined by the meta-material geometry; z is the direction of the wires; and k_z is a component of the wave vector along the wires. As it can be seen, the permittivity tensor is uniaxial, which reflects the

highly anisotropic geometry of the wire medium. Notably, it has been recently shown that in the electrostatic limit $\omega_0 = 0$, the effect of the wire medium results in the spherically symmetrical screening of the Coulomb potential. Namely, it has been shown [14] that potential $\phi(r)$ created by the charge Q is given by

$$\phi(r) = Qe^{-k_p r}/r, \quad (2)$$

coinciding with the screened Coulomb potential in isotropic plasma. For this reason, the wire medium has properties similar to those of plasma systems, namely, the potential is described by the Yukawa formalism [15]. Yukawa screening is a phenomenon in which the electric field produced by a charged particle is attenuated as it passes through a medium. This attenuation is caused by the interaction of the electric field with the medium, which contains other charged particles that can respond to the field. In our case, shielding is realized via surface density of free electrons on the wires. The shielding effect is important in understanding the behavior of atoms in electric fields; particularly, it plays a role in condensed matter physics [16] and plasma physics [17], including interaction between charged particles [18]. As is mentioned in our manuscript, we proposed wire medium as a platform for realization of artificial plasma with screening depth defined by geometrical parameters. In particular, we validate a spherically symmetrical potential profile experimentally and show that the measurement of the electrostatic E field can be used for precise determination of the effective plasma frequency.

II. FINITE LAYER APPROACH

While Eq. (2) may be adequate for the description of an infinite wire medium, the finite size effects should definitely substantially modify the shape of the potential. Indeed, the wire medium is an ideal uniaxial conductor, and thus when a probe charge is placed inside a wire medium, there should emerge a surface charge suppressing the the electric field inside the medium. At the same time, since the metamaterial is conducting only along one direction, the field will not be

^{*}evgeniy.koreshin@metalab.ifmo.ru

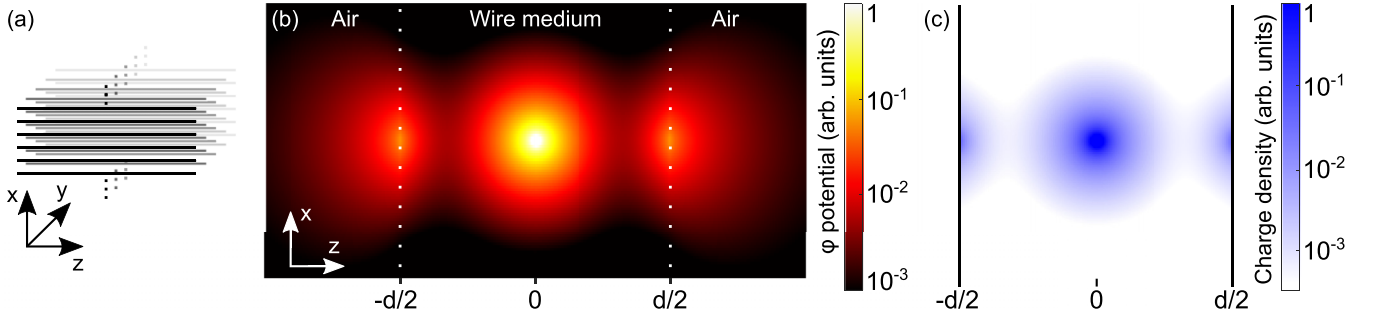


FIG. 1. (a) Geometrical problem concerning an unbounded layer in the xy plane composed of wires with finite length. (b) Analytically obtained potential distribution produced by the probe charge centered in the wire medium layer, dotted lines are boundaries. (c) Charge density distribution inside the layer.

totally suppressed. In order to get the quantitative distribution of potential and electric field in a finite slab of wire medium, one needs adequate boundary conditions (BC) for the displacement and field at the wire edges. While there were several suggestions for additional BC for the wire medium surface [19,20] for electromagnetic fields, they cannot be used in the electrostatic limit since they do not account for the charge accumulation at the surface of the metamaterial slab. We derive a BC which accounts for the surface charge accumulation and check its validity experimentally. One of the consequence of the surface charge accumulation is the nonmonotonous profile of the potential produced by a point charge, as shown in Fig. 1(b).

In order to obtain the expressions for the potential distribution, we consider an infinite slab consisting of finite-length wires. The slab thickness coinciding with the the wires length is d . The z axis is aligned with the wires, and assumes that the probe charge Q is placed in the center. To find the potential distribution we need to solve the Poisson equation

$$\text{div}[\hat{\epsilon} \nabla_{\mathbf{r}} \phi(\mathbf{r}, \mathbf{r}')] = 4\pi Q \delta(\mathbf{r} - \mathbf{r}'), \quad (3)$$

where $\hat{\epsilon} = 1$ equals 1 for $|z| > d/2$ and is given by the Fourier transform of Eq. (1) otherwise. The plasmonic wave vector k_p reads [21]

$$k_p^2 = \frac{2\pi/a^2}{\log(a/2\pi r_0) + 0.5275}, \quad (4)$$

where a is a period of the structure and r_0 is the radius of the wires.

We assume that the charge is inside the wire medium and want to obtain the potential distribution in all space. We first exploit the translational symmetry of the problem in the xy plane and take the Fourier transform along the x and y axes. The resulting one-dimensional differential equation can be further solved separately in three regions, $z > d/2$, $|z| < d/2$, $z < -d/2$. After applying the condition that the potential should decay at $z \rightarrow \pm\text{infinity}$, we are left with four unknown coefficients $A_{\mathbf{q}}$, $B_{\mathbf{q}}$, $C_{\mathbf{q}}$, $D_{\mathbf{q}}$ corresponding to the potential decaying exponentially in the outer regions, and two amplitudes inside the wire medium. Therefore, one needs two BC at each boundary to unambiguously define the potential. It should be noted that unlike the electrodynamical case, there is no additional wave inside the wire medium and thus additional BC is not required. The first [eq. (5)] BC is the continuity of the tangential components of the electric field, i.e., $\partial\phi/\partial x$

should be continuous at $z = \pm d/2$. The second BC [Eq. (6)] corresponds to the continuity of the normal component of the electric displacement field.

$$E_{x,y}^{\text{in}}(z = \pm d/2) = E_{x,y}^{\text{out}}(z = \pm d/2), \quad (5)$$

$$D_z^{\text{in}}(z = \pm d/2) = D_z^{\text{out}}(z = \pm d/2), \quad (6)$$

where indexes *in* and *out* correspond to location inside and outside the wire medium (WM) boundary, respectively. The electric displacement field having the nonlocal nature of permittivity is given by

$$\begin{aligned} D_z^{\text{in}} &= \int_{-d/2}^{d/2} dz'' \hat{\epsilon}_{zz}(z - z'') \partial_{z''} \phi_{\mathbf{q}}(z'', z'), \\ \hat{\epsilon}_{zz}(z - z') &= \frac{1}{2\pi} \int dk_z e^{-ik_z(z-z')} \epsilon_{zz}(\mathbf{k}) \\ &= \delta(z - z') - \frac{k_p^2}{2} |z - z'|, \end{aligned} \quad (7)$$

where $\hat{\epsilon}_{zz}(z - z')$ is the Fourier transform of the z component of Eq. (1), $|z|, |z'| < d/2$. The Fourier transform can be taken analytically, and the displacement can be algebraically expressed via the unknown amplitudes. Due to the spatial dispersion of the medium, a charge of the same sign as the probe charge is induced at the ends of the wires. The presence of such a surface charge density forces us to write the boundary condition in the form of Eq. (6), where the presence of induced charges on the interface of the medium is taken into account in the vector D , and since there are no external charges at the ends of the wires, the normal component of the field D must be continuous.

In order to find the distribution of potential, it is convenient to write explicitly partial waves which are produced by the probe charge and boundaries in the ansatz:

$$\begin{aligned} \phi_{\text{in}} &= 2\pi Q \sum_{k_x, k_y} e^{ik_x(x-x')} e^{ik_y(y-y')} \\ &\times \left[\frac{e^{-|z-z'|\kappa}}{\kappa} + A_{\mathbf{q}}(k_x, k_y) e^{-\kappa z} + B_{\mathbf{q}}(k_x, k_y) e^{\kappa z} \right], \\ \phi_{\text{out}}^{\text{up}} &= 2\pi Q \sum_{k_x, k_y} e^{ik_x(x-x')} e^{ik_y(y-y')} C_{\mathbf{q}}(k_x, k_y) e^{-q(z-d/2)}, \\ \phi_{\text{out}}^{\text{down}} &= 2\pi Q \sum_{k_x, k_y} e^{ik_x(x-x')} e^{ik_y(y-y')} D_{\mathbf{q}}(k_x, k_y) e^{q(z+d/2)}, \end{aligned} \quad (8)$$

where A_q, B_q, C_q, D_q are partial waves produced by boundaries and $q^2 = k_x^2 + k_y^2$ is the in-plane wave vector, $\kappa^2 = q^2 + k_p^2$.

Using this ansatz and the material property [Eq. (7)] of wire medium, we can rewrite both boundary conditions as

$$\begin{aligned} e^{-d\kappa/2} + \kappa A e^{-\kappa d/2} + \kappa B e^{\kappa d/2} &= \kappa C, \\ e^{-d\kappa/2} + \kappa B e^{-\kappa d/2} + \kappa A e^{\kappa d/2} &= \kappa D, \\ A\kappa e^{-\kappa d/2} - B\kappa e^{\kappa d/2} + e^{-\kappa d/2} + \frac{k_p^2}{\kappa}(A+B)\text{sh}(\kappa d/2) - \frac{k_p^2 d}{2}(Ae^{\kappa d/2} + Be^{-\kappa d/2}) + \frac{k_p^2}{\kappa^2}[1 - (1 + \kappa d/2)e^{-\kappa d/2}] &= qC, \\ A\kappa e^{\kappa d/2} - B\kappa e^{-\kappa d/2} - e^{-\kappa d/2} - \frac{k_p^2}{\kappa}(A+B)\text{sh}(\kappa d/2) + \frac{k_p^2 d}{2}(Ae^{-\kappa d/2} + Be^{\kappa d/2}) - \frac{k_p^2}{\kappa^2}[1 - (1 + \kappa d/2)e^{-\kappa d/2}] &= -qD. \end{aligned}$$

Now we can find the Fourier transform for all amplitudes:

$$\begin{aligned} A &= \frac{1}{\kappa} \frac{k_p^2 - e^{-\frac{1}{2}\kappa d}[\kappa(q + \frac{1}{2}k_p^2 d) - q^2]}{e^{-\frac{1}{2}\kappa d}[\kappa(q + \frac{1}{2}k_p^2 d) - q^2] + e^{\frac{1}{2}\kappa d}[\kappa(q + \frac{1}{2}k_p^2 d) + q^2]}, \\ B &= A, \\ C &= \frac{1}{\kappa} \frac{2[q^2 + k_p^2 \text{ch}(\frac{1}{2}\kappa d)]}{e^{-\frac{1}{2}\kappa d}[\kappa(q + \frac{1}{2}k_p^2 d) - q^2] + e^{\frac{1}{2}\kappa d}[\kappa(q + \frac{1}{2}k_p^2 d) + q^2]}, \\ D &= C. \end{aligned} \quad (9)$$

This allows to analytically solve the equation for the amplitudes and yields the final expression for the potential

$$\phi_{\text{in}}(\rho, z, \rho', z' = 0) = \frac{Q e^{-k_p|r-r'|}}{|r-r'|} + Q \int dq J_0(q|\rho - \rho'|) \frac{q}{\kappa} \left[\frac{2\{k_p^2 - e^{-\frac{1}{2}\kappa d}[\kappa(q + \frac{1}{2}k_p^2 d) - q^2]\}}{e^{-\frac{1}{2}\kappa d}[\kappa(q + \frac{1}{2}k_p^2 d) - q^2] + e^{\frac{1}{2}\kappa d}[\kappa(q + \frac{1}{2}k_p^2 d) + q^2]} \right] \cosh(\kappa z), \quad (10)$$

$$\phi_{\text{out}}^{\text{up}}(\rho, z, \rho', z' = 0) = Q \int dq J_0(q|\rho - \rho'|) \frac{q}{\kappa} \frac{2[q^2 + k_p^2 \cosh(\frac{1}{2}\kappa d)]}{e^{-\frac{1}{2}\kappa d}[\kappa(q + \frac{1}{2}k_p^2 d) - q^2] + e^{\frac{1}{2}\kappa d}[\kappa(q + \frac{1}{2}k_p^2 d) + q^2]} e^{-q(z-d/2)}. \quad (11)$$

The expression is written for the particular case when the probe charge is placed in the center of the slab ($z' = 0$). The results of Eqs. (10) and (11) are plotted in Fig. 1(b). As can be seen, while in the bulk of the structure the potential of the finite slab almost coincides with that of the infinite structure, in the vicinity of the boundary the potential is nonmonotonous, with a local minimum close to the boundary and a local maximum exactly at the boundary. The nonmonotonous behavior of the potential is due to the volumetric charge density induced by the probe charge. Figure 1(c) shows charge density distribution inside the layer obtained as $\nabla^2 \phi_{\text{in}}(x, z, y = 0)$, while $\nabla^2 \phi_{\text{out}}^{\text{up,down}}(x, z, y = 0) = 0$. As can be seen, a volumetric charge of the opposite sign is concentrated in the region of the probe charge, which provides shielding. The finite size of the medium results in a significant influence of the boundaries on the charge distribution within the layer, expressed as an increase in the charge density near the boundary and a local minimum in the middle. As a result, the electric field component along the wires changes sign [Fig. 2(b)], caused by the minimum of potential inside the layer [Fig. 2(a)].

III. EXPERIMENTAL MEASUREMENTS

The theoretical predictions have been validated experimentally through the electric field measurements along and across

the wires. The static electric field meter $\Pi 3 - 80 - E$ [22] [Fig. 3(a)] was arranged as an asymmetric metal plate rotated with a constant frequency around a certain axis. The stationary metal disk was located below. Both parts were connected to the signal amplifier. As a result, the modulated electrostatic field was processed as an ac signal by an Ecophysics-110A

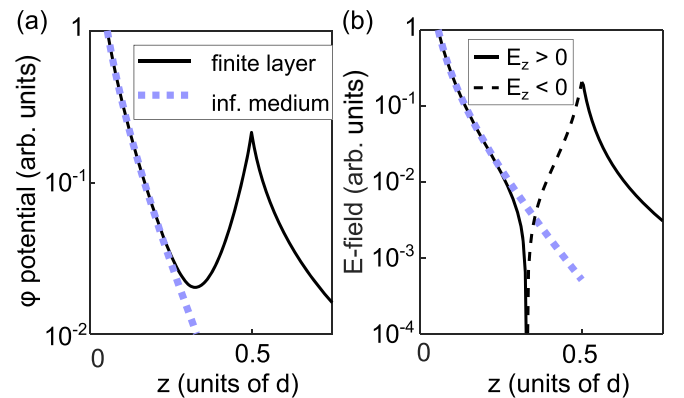


FIG. 2. (a) Electrostatic potential and (b) E field along the layer depth. Potential experiences the local maximum at the boundary, which leads to a reversal E-field [dashed line in (b)] far from the probe charge. The blue lines are the infinite wire medium solutions.

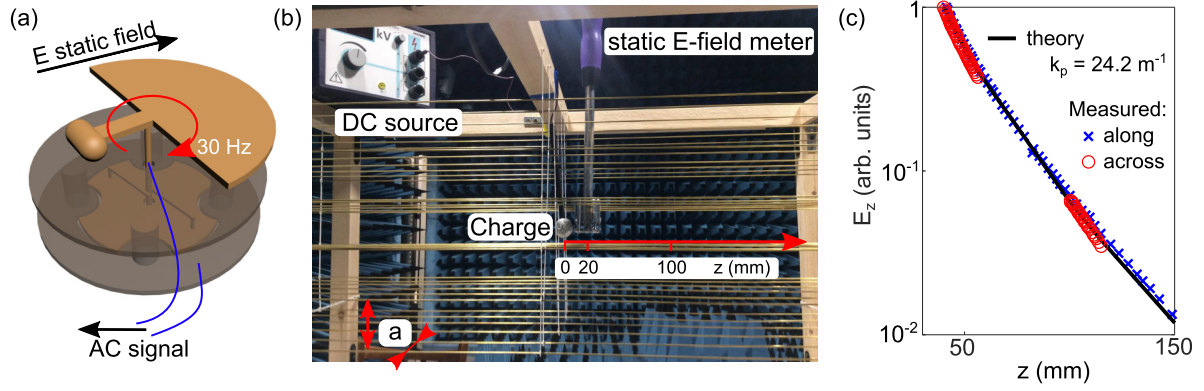


FIG. 3. Experimental details. (a) E-field meter interior; the rotating top and the stationary base are connected to the ac processing device. (b) Measurement setup consists of the wire medium sample ($a = 60$ mm), a probe charge, a dc voltage source, and the E-field meter. (c) Measured E field along and across the wires compared to theoretical results [Eq. (2)] for the best-fit parameter k_p case [Eq. (12)].

device [22]. The resulting device measured the average E field as $|\mathbf{E}| = \sqrt{E_x^2 + E_z^2}$, where $x - z$ is the rotational plane. The absolute value of the E field is normalized by the reference charges of the manufacturer. The instrumental error of the device is claimed as $\pm 15\%$. A three-dimensional (3D) scanner was used to move the E-field meter.

The experimental sample is an array of 8×6 wires with a length of 1 m [Fig. 3(b)] and radius $r_0 = 1$ mm. The distance between the adjacent wires was $a = 60$ mm. The wires were attached to a wooden frame using thin plastic holders that did not conduct electric current and showed a relatively small ability to accumulate a surface charge. The source of the electrostatic field was a metal ball with a radius of 10 mm with a potential of 2 kV relative to the grounding of the device, which was created by a constant voltage source [Fig. 3(b)]. The probe charge was placed in the center of the wire medium and was taken as the origin of the coordinate system.

In the case of measurements along the wires $\mathbf{E}(z, x = 0) = E_z$, the component E_x is zero due to the symmetry of the sample and the excitation. We also performed measurements across wires $\mathbf{E}(x, z = 0) = E_x$ inside four unit cells separately. In the last case, continuous movement is not possible since the E-field meter has to cross the wires. In order to carry out measurements in an adjacent cell, the device anchored on the 3D scanner was removed from the sample, shifted behind the wire, and placed back inside.

Figure 2(c) shows the experimentally obtained electric field along and across the wires near the probe charge, which appeared to be the same as theoretically proposed [14]. In order to estimate the attenuation factor defined by the plasma wave vector, we compare the analytical results for the given k_p with the measured E field in terms of minimum of normalized deviation σ , as follows:

$$\sigma(k_p) = \sum_{i=1}^N \sqrt{\left[\frac{E_{\text{meas}}(r_i) - E_{\text{th}}(r_i, k_p)}{E_{\text{th}}(r_i, k_p)} \right]^2} \quad (12)$$

where E_{meas} is the measured value of the field at a distance of r_i from the probe charge, E_{th} is that given by $\nabla\phi(r_i, k_p)$ from Eq. (2). The parameter $\sigma(k_p)$ quantitatively shows how analytical E-field distribution with certain k_p describes measured data. The value of k_p which corresponded to the minimum

$\sigma(k_p)$ was assumed as the resulting one. According to this technique, we found k_p parameters along and across the wires, which values are equal 24.4 and 24.2 m^{-1} , respectively. The analytical value of Eq. (4), which depends only on geometrical parameters, is 25 m^{-1} .

At the next step we compared the measurement in the entire spatial region E field (Fig. 4) along and across the wires set with the analytically obtained ones. The results show that the theoretical approach is fully confirmed by the measurements across the wires direction [Fig. 4(a)]. In the direction along the wires [Fig. 4(b)], the absolute value of the E field decreased to the noise level of the measuring device (0.2 kV/m) and increased from 220 mm to the boundary. Such a discrepancy could be related both to the accuracy of the experiment and to an unsuitable BC for a particular direction.

IV. PLASMA FREQUENCY EXTRACTION

The plasma frequency can be determined from the experimentally obtained wave vector, $f_p = Ck_p/2\pi$, as 1.165 GHz, which is in proper agreement with both theoretically obtained 1.196 GHz and numerically obtained 1.175 GHz. In the last

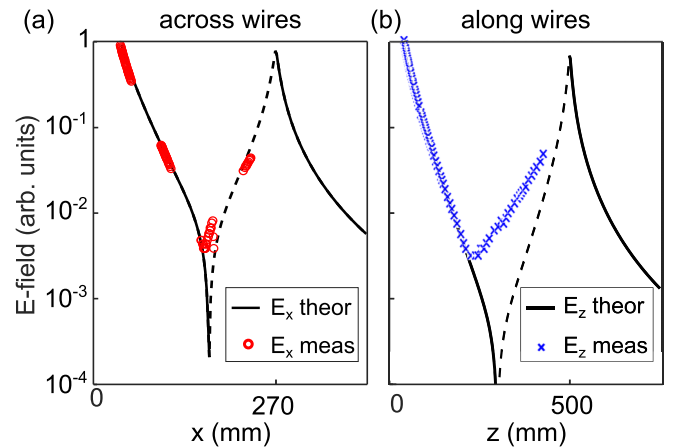


FIG. 4. E-field distribution obtained experimentally (a) across and (b) along the wires. Solid and dashed lines are given by Eq. (10) for layer thickness $D = 570$ and 1000 mm corresponding to the sample size.

case, the plasma frequency was calculated directly using the CST Microwave Studio eigenmode solver as well as the full-wave simulation.

It should be noted that the distance between the probe charge and a measurement point is required to be given precisely, which means that both parts are negligibly small. However, in the experimental setup we measured the distance between the surfaces of the charge and the E-field meter. In order to compensate for the finite size of components, we added the sum of the meter and the charge radii 27 mm to the distance. For verification, we carried out several measurements with different initial distances and obtained relevant agreement in results: 24.3, 24.8, and 24.3 m⁻¹ for measurements along the wires, and 24.2 and 25.3 m⁻¹ for those across them.

V. CONCLUSION

In this article we have performed the measurements of the electrostatic E field produced by a probe charge

immersed in a wire medium. We experimentally confirmed the spherically symmetrical potential profile in the anisotropic medium. Moreover, for a 60 × 60-mm array of 1-mm-thick wires we experimentally obtained the plasma frequency of 1.165 GHz by electrostatic measurements, which are in proper agreement with both the theoretical (1.196 GHz) and numerical (1.175 GHz) approaches. Finally, the boundary condition in the finite slab was theoretically predicted and experimentally demonstrated to result in a nonmonotonous potential profile of the Coulomb interaction.

ACKNOWLEDGMENTS

The authors thank Denis Sakhno for helpful discussions. The work was supported by a grant for scientific school HIII-2359.2022.4. E.K. acknowledges the RPMA grant from the School of Physics and Engineering of ITMO University. The authors acknowledge support from the Russian Science Foundation (Grant No. 20-79-10316).

-
- [1] N. S. Rytova, *Moscow University Physics Bulletin* **3**, 30 (1967).
 - [2] L. V. Keldysh, *Sov. J. Exp. Theor. Phys. Lett.* **29**, 716 (1979).
 - [3] P. Cudazzo, I. V. Tokatly, and A. Rubio, *Phys. Rev. B* **84**, 085406 (2011).
 - [4] A. Chernikov, T. C. Berkelbach, H. M. Hill, A. Rigosi, Y. Li, B. Aslan, D. R. Reichman, M. S. Hybertsen, and T. F. Heinz, *Phys. Rev. Lett.* **113**, 076802 (2014).
 - [5] P. Gaddam and W. Ducker, *Langmuir* **35**, 5719 (2019).
 - [6] L.-C. Cheng, S. L. Kuei Vehusheia, and P. S. Doyle, *Langmuir* **36**, 3346 (2020).
 - [7] S. E. Seo, M. Girard, M. O. De La Cruz, and C. A. Mirkin, *ACS Cent. Sci.* **5**, 186 (2019).
 - [8] J. C. Everts, B. Senyuk, H. Mundoor, M. Ravnik, and I. I. Smalyukh, *Sci. Adv.* **7**, eabd0662 (2021).
 - [9] J. P. de Souza and M. Z. Bazant, *J. Phys. Chem. C* **124**, 11414 (2020).
 - [10] N. I. Zheludev and Y. S. Kivshar, *Nat. Mater.* **11**, 917 (2012).
 - [11] M. Kadic, G. W. Milton, M. van Hecke, and M. Wegener, *Nat. Rev. Phys.* **1**, 198 (2019).
 - [12] C. R. Simovski, P. A. Belov, A. V. Atrashchenko, and Y. S. Kivshar, *Adv. Mater.* **24**, 4229 (2012).
 - [13] P. A. Belov, R. Marques, S. I. Maslovski, I. S. Nefedov, M. Silveirinha, C. R. Simovski, and S. A. Tretyakov, *Phys. Rev. B* **67**, 113103 (2003).
 - [14] I. Karakasoglu and S. Fan, *Phys. Rev. B* **93**, 075433 (2016).
 - [15] H. Yukawa, *Proc. Phys.-Math. Soc. Jpn.* **17**, 48 (1935).
 - [16] L. Banyai and S. Koch, *Z. Phys. B* **63**, 283 (1986).
 - [17] M. Rosenberg and G. Kalman, *Phys. Rev. E* **56**, 7166 (1997).
 - [18] G. M. Harris, *Phys. Rev.* **125**, 1131 (1962).
 - [19] M. G. Silveirinha, *IEEE Trans. Antennas Propag.* **54**, 1766 (2006).
 - [20] S. I. Maslovski, T. A. Morgado, M. G. Silveirinha, C. S. Kaipa, and A. B. Yakovlev, *New J. Phys.* **12**, 113047 (2010).
 - [21] P. A. Belov, S. A. Tretyakov, and A. Viitanen, *J. Electromagn. Waves Appl.* **16**, 1153 (2002).
 - [22] <https://www.octava.info/>.
- Correction:* The omission of a support statement in the Acknowledgment section has been fixed.